Surface-Enhanced Raman Spectroscopy of Benzenethiol Adsorbed from the Gas Phase onto Silver Film over Nanosphere Surfaces: Determination of the Sticking Probability and Detection Limit Time[†]

Kevin B. Biggs, Jon P. Camden, Jeffrey N. Anker, and Richard P. Van Duyne*

Northwestern University, Department of Chemistry, Evanston, Illinois 60208-3113

Received: December 20, 2008

A chemical warfare agent (CWA) gas detector based on surface-enhanced Raman spectroscopy (SERS) using robust nanostructured substrates and a portable Raman spectrometer is a promising alternative to existing modalities. A gas-dosing apparatus was constructed to simulate chemical gas exposure and provide a platform for quantitative analysis of SERS detection. As a first step toward characterizing SERS detection from the gas phase, benzenethiol (BT) has been chosen as the test analyte. SERS spectra were monitored during BT adsorption onto a silver film over a nanosphere (AgFON) substrate. The SERS detection limit time (DLt) for BT on a AgFON at 356 K is found to be 6 ppm-s (30 mg-s m^{-3}) for a data acquisition time (t_{acq}) of 1 s. The DLt for this kinetically controlled sensor is fundamentally determined by the low sticking probability of BT on AgFONs which is determined to be ~2 × 10^{-5} at 356 K. The sticking probability increases with increasing temperature consistent with an adsorption activation barrier of ~13 kJ mol^{-1}. Although the DLts found in the present study for BT are in the low ppm-s, a theoretical model of SERS detection indicates DLts below 1 ppb s^{-1} for t_{acq}= 1 s are, in fact, achievable using existing portable Raman instrumentation and AgFON surfaces. Achieving this goal requires the sticking probability be increased 3 orders of magnitude, illuminating the importance of appropriate surface functionalization.

Introduction

Development of a robust, rapid, and sensitive detector for chemical warfare agents (CWAs) released in the air is a necessity on the battlefield and constitutes an important analytical challenge. The LCt$_{50}$ refers to the product of the CWA concentration in air and time required to kill 50% of an unprotected population by inhalation during acute exposure. The LCt$_{50}$ for mustard gas (HD) and nerve agent VX, one of the most lethal CWAs, is 290 ppm-min and 910 ppb-min, respectively.[1,2] Although HD has a faint smell (odor threshold of 120 ppb),[3] many agents like VX are odorless. Chronic exposure to CWAs also poses a serious threat, as they can remain in the environment for months.[1,4,5]

Presently, there are a number of competing technologies for the detection of chemical agents in the gas phase. All detection modalities deviate from the ideal in their capacity to optimize factors such as size, cost, sensitivity, speed, specificity, accuracy, reversibility, and reusability. Chemically doped detection papers, such as U.S. military M8 strips, are inexpensive, portable, and easy to use but relatively insensitive, nonspecific, and prone to false positives. Field-portable gas chromatography mass spectroscopy (GC MS) instruments are sensitive and specific but expensive and require long sampling times.[6,7] Ion-mobility spectrometry (IMS) is currently the leading technology for chemical sensing.[8–11] Using a portable mobility spectrometer, Zimmerman et al. reports identification of 34 μg m^{-3} and 3 μg m^{-3} for HD and VX gas, respectively, in just a few seconds (~20 ppb-s and ~820 ppt-s, respectively).[12] Although, IMS provides rapid analysis in a compact package, there is no potential for remote sensing, and complex mixture identification
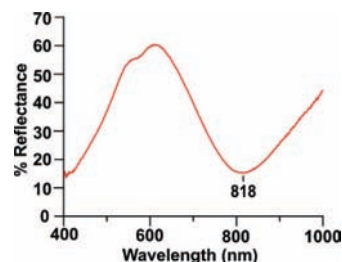

Figure 1. The localized surface plasmon resonance of a AgFON surface optimized for SERS with 785 nm laser excitation wavelength.

is challenging. Also the destructive nature of IMS makes analyte preconcentration difficult resulting in little improvement in the detection limit upon further exposure.

Raman spectroscopy is an attractive alternative to conventional sensing modalities. As a vibrational spectroscopy, Raman spectroscopy has narrow line width and the ability to distinguish between molecules of great similarity. Raman scattering cross-sections are generally small, on the order of 10^{-30} cm^2 molecule^{-1} sr^{-1}, 14 orders of magnitude less than those of fluorescence.[13] This limited signal can be overcome using SERS. SERS is characterized by large enhancements in the effective Raman cross-section (typically 10^5–10^8) of analytes spatially confined within the electromagnetic fields (viz., 0–4 nm) generated upon excitation of the localized surface plasmon resonance (Figure 1) of metal nanostructured surfaces. SERS detection is rapidly progressing and has found applications in biomedicine,[14–18] environmental analysis,[19–21] and surface science.

SERS detection of hazardous gases has been reported previously.[22,23] SERS detection of half-mustard gas, a mustard simulant, was reported using a portable Raman spectrometer

---

and AgFON substrate.[24] Nerve agent simulants, dimethyl methylphosphonate and diisopropyl methylphosphonate, have been detected by SERS in the gas phase using electrochemically roughened silver oxide substrates.[25,26] However, a quantitative approach toward SERS gas detection, where the physical parameters of detection are determined and implemented into a comprehensive model, has remained absent from the literature. SERS analysis of organothiols is an attractive case study for such an analysis with numerous comparative studies provided by the self-assembled monolayer (SAM) and molecular electronics communities.[27−34] BT was chosen, specifically, as a test analyte for SERS gas detection analysis because of its ability to form well ordered SAMs from the gas phase with strong S−Ag bonds (∼167 kJ mol^{−1}).[35−41] Also the S−Ag bond is irreversible under ambient conditions and likely responsible for the observed irreversible binding of half-mustard gas to the AgFON substrate.[24] Furthermore, BT has a large UV absorption cross-section which provides a convenient means for monitoring its concentration in the gas phase by UV−vis spectroscopy.[42]

Experimental Methods

Materials. All chemicals were reagent grade and used as received. Oxygen-free high-conductivity copper was obtained from McMaster-Carr (Chicago, IL) and cut into 18 mm diameter disks. Surfactant-free, silica nanosphere suspensions (600 nm ± 20 nm 10% solid) were purchased from Interfacial Dynamics. Ultrapure water (18.2 MΩ cm^{−1}) from a Millipore system (Marlborough, MA) was used for substrate and solution preparation. Silver wire (99.99%) was purchased from Kurt J. Lesker Co. BT was purchased from Aldrich (Milwaukee, WI). NH$_4$OH and H$_2$O$_2$ were purchased from Fisher Scientific (Fairlawn, VA) and CH$_3$CH$_2$OH from Pharmco-AAPER and used for cleaning.

AgFON Fabrication. Copper substrates were cleaned by sonication (1510 Branson ultra sonicator) in 10:1:1 H$_2$O:30% H$_2$O$_2$:NH$_4$OH. Ten microliters of nanosphere solution was drop-coated onto a clean copper substrate and allowed to self-assemble at room temperature. Ag films (200-nm thick) were then deposited at a rate of 2 Å s^{−1} under high vacuum (5.0 × 10^{−7} torr) over the nanosphere-covered surface using a thermal vapor deposition system (home-built).[43,44] The Ag mass thickness and deposition rate were measured by a 6-MHz gold-plated quartz crystal microbalance purchased from Sigma Instruments (Fort Collins, CO).

Surface-Enhanced Raman Spectroscopy. A portable Raman spectrometer purchased from DeltaNu (Laramie, WY, Inspector Raman) was used to record SERS spectra. Excitation is achieved at 785 nm (diode laser) with a spot size full width half-max (fwhm) of ∼30 μm. Spectra were taken at 2 mW and t_{acq}= 1 s in a 180° backscattering geometry. According to manufacturer specifications, the solid angle of collection, Ω, is 0.30 steradians, the detector quantum efficiency, $Q(\omega_s)$, is ∼25% in the region of interest, and the transmission efficiency of the collection optics, T_o, and spectrometer, T_m, is 70% and 80%, respectively.

UV−vis Spectroscopy. Spectra were acquired using a Mikropack DH2000 Deuterium-Halogen light source fiber coupled (Ocean Optics QP400-2-SR and QP600-2-SR) to an Ocean Optics HR4000 high-resolution spectrometer taken with t_{aqu} = 20 ms and 10^3 averages. The UV flow cell used measured 10.9 cm in length. The UV−vis cross-section of BT was determined to be 7.4 × 10^3 L cm^{−1} mol^{−1}, by calculating the slope (R^2 = 0.997) of a Beer's law plot including five different concentrations of BT in cyclohexane.
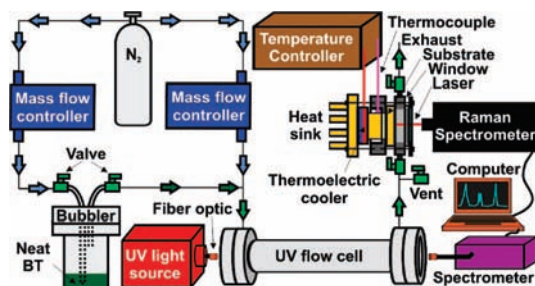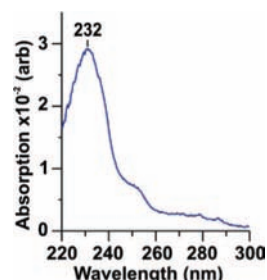

Figure 2. Gas-phase dosing apparatus.

Figure 3. UV spectra of BT gas acquired during dosing.

Dosing. Gas dosing is achieved by mass flow-controlled (MKS, M100BO1312CR1BV) mixing of BT saturated N$_2$ with pristine N$_2$ (Figure 2). The saturated BT carrier gas is passed at 1 mL min^{−1} through a bubbler containing neat BT and is later diluted downstream at 100 mL min^{−1}. BT concentration is monitored by UV−vis spectroscopy (Figure 3). Once the BT concentration reaches steady state, the gas stream is allowed to flow over the SERS substrate by opening the back valve on the sample cell and then simultaneously opening and closing the front and vent valve, respectively. Only ultradry grade N$_2$ was used. All piping is 0.25 in. stainless steel except the sample cell which is 0.125 in. All connections are made with standard Swagelock or VCR fittings.

Temperature Control. A Peltier solid-state thermoelectric cooler (Melcor, CP 1.0−31−05 L) controlled by a Melcor MTTC-1410 temperature controller (±0.004 C) was used for temperature control. A temperature sensor (Melcor, 2-wire PT1000 RTD) in contact with a copper cylinder (length 8 mm diameter 10 mm) clamped between the TEC and substrate provide temperature feedback. Silicon-based grease (Radio Shack) was applied at the TEC/copper cylinder junction and copper cylinder/substrate junction.

Analysis. Spectra were stored on a hand-held computer. All spectra were processed with Matlab scripts which calculated the peak intensities by subtracting the maximum peak height from the minimum in a baseline region. A conversion factor, C, was determined for converting SERS intensities recorded in adu mW[−1] s^{−1} to photons detected using benzene (BZ) as a standard and the general expression:[45]

$$I(\omega_s) = I(\omega_L)N\frac{d\sigma(\omega_s)}{d\Omega}Z \qquad (1)$$

where $I(\omega_s)$ is the Raman scattering intensity at ω_s, $I(\omega_L)$ is the incident laser intensity at ω_L, N is the number density of scatters, $(d\sigma(\omega_s))/(d\Omega)$ is the Raman cross-section at ω_s, and Z is a geometric factor that takes into account the spectrometer depth of field. C is calculated by modification of eq 1 to account for t_{acq} and some experimental parameters:

Surface-Enhanced Raman Spectroscopy of Benzenethiol

J. Phys. Chem. A, Vol. 113, No. 16, 2009 **4583**

$$C = I(\omega_L)N_{BZ}\frac{d\sigma_{BZ}(\omega_s)}{d\Omega}t_{acq}\Omega T_m T_o Q(\omega_s)I_R^{BZ}(\omega_s)^{-1}\int I_s^{BT}(\omega_s, Z)dZ$$

$$(2)$$

where $(d\sigma_{BZ}(\omega_s))/(d\Omega)$ is the BZ Raman cross-section (4.9×10^{-30} cm^2 sr^{-1} molecules^{-1} at $\omega_s = 992$ cm^{-1})[46] and $I_R^{BZ}(\omega_s)$ is the BZ Raman scattering intensity (adu mW^{-1} s^{-1}) at ω_s. The geometric factor, $\int I_s BT(\omega_s, Z)dZ$, was determined by collecting a series of BT SERS spectra on a AgFON at $\omega_s = 1076$ cm^{-1}, as a function of focal distance, z (150 μm steps, Line Tool Co. Model A RH micro positioning stage). Normalization and integration of peak intensities yields $z = 0.12$ cm. The conversion factor was determined to be 32 photons mW s adu^{-1}.

The Raman cross-section of BT, $(d\sigma_{BT}(\omega_s))/(d\Omega)$, at $\omega_s = 1091$ cm^{-1} (mode responsible for SERS at 1076 cm^{-1}) was determined to be 6.4×10^{-31} cm^2 sr^{-1} molecule^{-1} by comparison with the known BZ Raman cross-section using the relation:

$$\frac{d\sigma_{BT}(\omega_s')}{d\Omega} = \frac{I_R^{BT}(\omega_s')}{I_R^{BZ}(\omega_s)} \times \frac{N_{BZ}}{N_{BT}} \times \frac{d\sigma_{BZ}(\omega_s)}{d\Omega} \qquad (3)$$

where $I_R^{BT}(\omega_s)$ is the Raman scattering intensity of neat BT at ω_s.

Results and Discussion

An important property of this gas-phase SERS study is that BT binds irreversibly to the SERS substrate through a strong S–Ag bond. Similarly, many CWAs can irreversibly bind to silver or chemically functionalized silver surfaces, and the S–Ag bond is likely responsible for the observed irreversible binding of mustard gas to the AgFON substrate. As a result of irreversible adsorption, detection here is characterized, not by a limit of detection, but by a detection limit time (DLt) dependent on the kinetic rate of analyte adsorption. Lower concentrations can be detected for longer exposure periods, and the DLt is defined as the minimum concentration that can be detected in one second of exposure for a $t_{acq} = 1$ s and spot size of 1.4×10^{-5} cm^2. This study seeks to discover how quickly molecules can be detected by SERS and how it might be accelerated.

To quantitatively characterize SERS gas detection, the SERS signal arising from 8 ppm (40 mg m^{-3}) BT gas in N$_2$ dosed to a AgFON maintained at 358 K was continuously monitored with a portable Raman instrument (Figure 4A). A comparison of the SERS and normal Raman spectra of BT is shown in Figure 4B, with slight deviations in peak position highlighted. Shifts in peak position are commonly observed in SERS and arise from differences in the chemical environment experienced by the bound and neat species. Differences in relative SERS and normal Raman peak intensities are attributed to preferential enhancement of vibration modes oriented perpendicular to the surface.[40,47,48]

The temporal evolution of the BT SERS intensity at 1076 cm^{-1} is shown in Figure 5A. The DLt here is determined by analyzing the background noise prior to chemical dosing and assessing when a measurable SERS signal is observed. The initial rate of adsorption is illustrated by the slope of the red line in Figure 5A, determined by a linear regression fit to the first four data points in the linear regime of the adsorption uptake curve, yielding $k = 8.2 \times 10^4$ photons s^{-1} ($R^2 > 0.999$). This
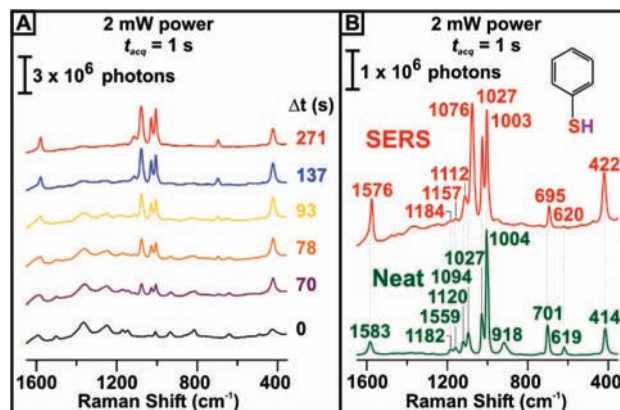

Figure 4. (A) SERS acquired on a AgFON maintained at 358 K before and during exposure to 8 ppm BT gas. (B) The upper red trace is SERS of BT taken on a AgFON. For comparison, normal Raman of neat BT is shown in the lower green trace.
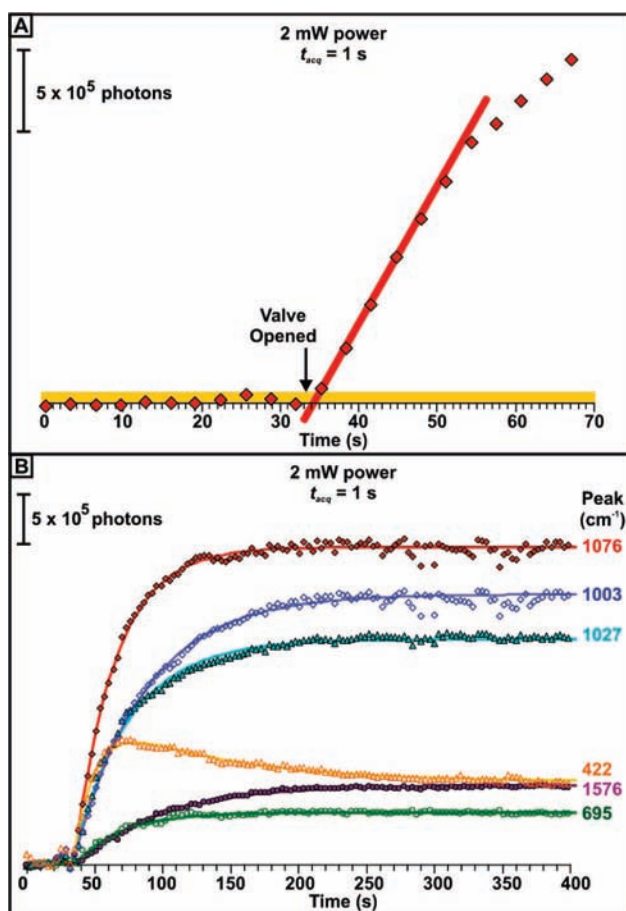

Figure 5. (A) The red line is a linear fit to the initial SERS intensity growth at 1076 cm^{-1} on a AgFON at 356 K. The gold region represents three standard deviations above the mean background noise. (B) All peaks grow according to first-order Langmuir kinetics except at 422 cm^{-1} which exhibits double exponential behavior.

slope can be easily converted into a rate of molecular adsorption, k_{ads}, through the following expression:

$$k_{ads} = \frac{kNA}{N_P^{sat}(\omega_s)} \qquad (4)$$

where N is the surface number density ($\sim 6.8 \times 10^{14}$ molecules cm^{-2} on flat Ag surfaces),[49] A is the AgFON surface area excited

(approximated by twice the planar area illuminated by the fwhm to account for AgFON morphology), and $N_P^{sat}(\omega_s)$ is the number of SERS photons detected at saturation coverage and frequency ω_s. The calculated rate is 2.5×10^8 molecules s^{-1}. The intersection of the linear fit with the detection threshold signal, represented by three standard deviations above the mean background signal ($\Delta = 5.7 \times 10^4$ photons), indicates the detection threshold is met following a 0.69 s dose. The SERS DLt is thus 6 ppm-s for BT gas adsorption on a AgFON maintained at 358 K using $t_{acq} = 1$ s. This detection threshold corresponds to 1.7×10^8 molecules, 280 attomoles, or 1.8% of a monolayer.

The sticking probability is the chance a molecule that collides with the substrate adsorbs. In characterizing the DLt the value of the sticking probability is most important in the initial, linear regime of adsorption, where the number of unoccupied sites are much greater than the number of occupied and adsorption occurs at a constant rate. A comprehensive model for determining the total SERS intensity detected based on this initial sticking probability has been previously formulated.[44] Incorporating the known parameters for the experimental setup used in this work and generalizing this model for the analyte Raman cross-section and t_{acq}, the number of SERS photons detected at ω_s, $N_P(\omega_s)$, can be expressed through the following relation during the initial linear regime of adsorption:

$$N_P(\omega_s) = 1.0 \times 10^{35} \text{ (molecules} \times \text{photons} \times \text{sr} \times$$
$$\text{cm}^{-2} \times \text{torr}^{-1} \times \text{s}^{-2}) \frac{d\sigma(\omega_s)}{d\Omega} P_i t_{exp} t_{acq} S_i \text{EF}(\omega_s) \quad (5)$$

where P_i is the partial pressure, t_{exp} is the chemical gas exposure time, S_i is the initial sticking probability, and $\text{EF}(\omega_s)$ is the enhancement factor at ω_s ($\sim 10^7$ for the AgFON at 1076 cm^{-1}),[49] defined as the increase in analyte Raman scattering cross-section observed upon adsorption to a SERS substrate.

The sticking probability for organothiols on noble metal surfaces has been shown to range from unity to 10^{-8}.[29,50,51] The initial sticking probability, S_i, is expressed as a ratio of the initial adsorption rate to the BT collision frequency, approximated using ideal gas kinetics:

$$S_i = k_{ads}\sqrt{2\pi MRT}[P_i AN_A]^{-1} \quad (6)$$

where M is the molar mass, R is the ideal gas constant, T is the temperature of the dosed gas, and N_A is Avogadro's number. Using eq 6 the BT sticking probability is calculated to be 1.5×10^{-5} (the BT surface collision rate is 3.7×10^{13} molecules s^{-1} at 297 K and 1 atm). Substitution of this sticking probability in eq 5 predicts $N_P(\omega_s) = 8.2 \times 10^4$ photons following a $t_{exp} = 1$ s of 8 ppm BT with $t_{acq} = 1$ s. Changing S_i to 0.01, a 3 orders of magnitude increase, increases $N_P(\omega_s)$ to 5.6×10^7 photons, requiring only $t_{acq} = 1$ ms for positive detection. A S_i of unity would decrease the DLt from the 6 ppm-s demonstrated here to 90 ppt-s with $t_{acq} = 1$ s.

Equations 5 and 6 suggest at least five methods to increase the adsorption kinetics and otherwise improve the DLt. One method is to increase the collisions frequency by artificially increasing the pressure of the gas being analyzed. It is expected that the collision rate may be increased by 3 orders of magnitude without excessive difficulty (for example 100–1000 atm pressure is often used in high performance liquid chromatography columns). A second method, commonly employed in GC, is to increase the concentration of analyte with the use of cold traps or solvent traps, and then flow a concentrated gas stream over the sample. A third method is to increase the sticking probability. Increasing the sticking probability may be achieved by modifying the surface to increase the interaction of the analyte with the surface. For this method to succeed, it will be important to systematically study the activation barriers to adsorption, for example by varying the substrate temperature. A fourth potential method is to ionize the analyte and use electric fields to direct the ions to the sensing region. Finally the DLt can be improved by increasing the signal-to-noise ratio through improvements in the spectrometer, substrate, and signal analysis. It is also apparent from eq 5 that $N_P(\omega_s)$ is directly proportional to enhancement factor. Model calculations predict SERS enhancement factors can reach values of $\sim 10^{11}$ in the junctions between nanoparticle dimers.[52,53] SERS active sites with an EF(ω_s) of 10^{11} covering 10% of the substrate surface could increase the number of photons detected independent of any increase in the kinetics of the adsorption process. In addition, the signal-to-noise ratio could be increased by addition of an appropriate SERS reference standard, which could be added through controlled gas-phase adsorption of a fraction of a monolayer.

The Raman cross-sections of several CWAs and CWA simulants have been measured by Christesen and show strongest lines on order 10^{-30} cm^2 sr^{-1} molecule^{-1} (at 785 nm excitation).[13] These Raman cross-sections are greater than that of the 1076 cm^{-1} BT peak, thus requiring even smaller enhancement factors to achieve similar SERS signals to those reported here. However, the sticking probabilities of these agents on AgFON surfaces are expected to be lower than that of BT.

With the exception of the 422 cm^{-1} mode, SERS peak growth appears to follow *time-dependent* Langmuir kinetics (Figure 5B), where coverage, θ, is described by:

$$\theta = \theta_{sat}[1 - \exp(-rt_{exp})]] \quad (7)$$

θ_{sat} represents saturation coverage and r is the rate constant for adsorption. The growth in intensity of the 422 cm^{-1} peak is best described by a double exponential with a risetime constant of 15 s, less than half the risetime of the other peaks, and decay time of 85 s. The 422 cm^{-1} mode's deviation from first-order Langmuir kinetics is likely related to its strong dependence on the α_{zz} tensor, i.e., its electromagnetic enhancement is very sensitive to surface layer orientation.[40] Assigned to the C–S stretching and ring in-plane deformation vibration,[39] the double-exponential behavior of the 422 cm^{-1} mode is consistent with a gradual reordering of the adsorbed layer as the surface approaches saturation coverage, a phenomena previously observed in BT and other organothiol adsorption studies.[28,32,34]

The temperature dependence of BT adsorption on a AgFON is shown in Figure 6A, where the 1076 cm^{-1} peak intensities have been normalized to a saturation coverage intensity of 3.6×10^6 photons, occurring at 1100 s for the 260 K data (not shown) for the purpose of comparison. A comparison of the slopes in Figure 6A reveal that the initial sticking probability increases exponentially with temperature and by a factor of 5 over the temperature range studied, from 1.5×10^{-5} to 2.8×10^{-6}, indicative of chemisorption.[54] The inset of Figure 6 illustrates the linear relation of the $\ln(k_{ads})$ plotted against $1/T$ with the activation energy determined using the Arrehnius equation.[55]

$$k_{ads} = Ae^{-E_a/RT} \quad (8)$$

Surface-Enhanced Raman Spectroscopy of Benzenethiol

J. Phys. Chem. A, Vol. 113, No. 16, 2009 **4585**

where A is the pre-exponential factor and E_a is the activation energy. The slope yields an activation energy barrier of 13 kJ mol^{-1}. This activation energy is comparable with those measured by Dubois et al. for the chemisorption of ethanethiol and methanethiol gas on Au (21−29 kJ mol^{-1}).[51] It is hypothesized that this activation energy is required for organothiol dissociative attachment (RSH + Au → RS/Au + $^1/_2$H$_2$). Further evidence of a dissociative attachment mechanism is in the disappearance of the of S−H in-plane bending vibrational mode[39] located at 918 cm^{-1}, absent in the SERS spectra (see Figure 4B). Contrary to the work of Dubois et al. and Eberhardt et al. with alkanethiol adsorption on Au(111), the data here does not indicate any physisorbed precursor state where the RSH remains intact on the surface before dissociation.[31,51] It is unclear whether this

difference in observed BT surface chemistry is related to a difference in the AgFON morphology compared with the of flat single crystal Au(111) surfaces used in these studies or whether the kinetics of BT adsorption differs from that of alkanethiol.

An unexpected, double-humped feature is apparent in the 297 and 260 K data sets, where an abrupt deviation from Langmuir kinetics is observed and BT exhibits presaturation increases in sticking probability (Figure 6B,C). Such adsorption dynamics have not been observed for alkanethiol adsorption from the gas phase on flat Au surfaces, and more work is needed to understand the physical nature behind these features.

Conclusions

The results presented represent a significant step toward the real-time gas detection of CWAs with portable SERS instrumentation. A study of BT gas-phase adsorption on AgFONs provides an instructive system for studying the limits of gas-phase SERS detection. The DLt's were determined by comparing the early temporal evolution of the BT SERS signal with respect to the background signal prior to dosing using $t_{aqu} = 1$ s. The SERS DLt for BT on a AgFON at 356 K is projected to be 6 ppm-s, with accumulation of analyte during extended exposer periods enabling detection of lower concentrations. The calculated initial sticking probability of $\sim 2 \times 10^{-5}$ for this system indicates the greatest improvements in SERS DLt's below 1 ppb-s, will be achieved through increases in adsorption kinetics. The initial BT/AgFON sticking probability is found to be strongly temperature dependent with an activation barrier of ~ 13 kJ mol^{-1}. The quantitative nature of these experiments has provided insight into the potential use of SERS as a gas-phase detection modality. Looking toward the future, highly enhancing SERS substrates with optimized surface/analyte affinities are poised to play an increasingly important role in areas where robust, sensitive, and affordable sensing is required.

Figure 6. (A) SERS intensity at 1076 cm^{-1} monitored on a AgFON at temperatures 358, 297, and 260 K. Linear regression lines, shown by the red, purple, and blue lines, are fit to the initial slope of each curve and plotted as ln rate (k_{ads}) vs 1/T. Slope yields an activation energy of ~ 13 kJ mol^{-1}. (B) SERS peaks monitored on a AgFON at 297 K and (C) 260 K.

References and Notes

(1) Toxicological Profile for Sulfur Mustard; U.S. Department of Health and Human Services, 2003.

(2) Holstege, C. P.; Kirk, M.; Sidell, F. R. Chemical Warfare: Nerve Agent Poisoning. *Crit. Care Clin.* **1997**, *13* (4), 19.

(3) Material Safety Data Sheet: Mustard Gas; U.S. Edgewood Chemical Biological Center, 1999.

(4) Adams, G. K.; Yamamura, H. I.; O'Leary, J. F. Recovery of Central Respiratory Function Following Anticholinesterase Intoxication. *Eur. J. Pharmacol.* **1976**, *38*, 101.

(5) Crenshaw, M. D.; Hayes, T. L.; Miller, T. L.; Shannon, C. M. Comparison of the Hydrolytic Stability of S-(N,N-diethylaminoethyl)isobutyl methylphosphonothiolate with VX in Dilute Solution. *J. Appl. Toxicol.* **2001**, *1*, 3.

(6) Smith, P. A.; Lepage, C. R. J.; Koch, D.; Wyatt, H. D. M.; Hook, G. L.; Betsinger, G.; Erickson, R. P.; Eckenrode, B. A. Detection of Gas-Phase Chemical Warfare Agents Using Field-Portable Gas Chromatography-Mass Spectrometry Systems: Instrument and Sampling Strategy Considerations. *TrAC, Trend. Anal. Chem.* **2004**, *23* (4), 10.

(7) Hook, G. L.; Lepage, C. R. J.; Miller, S. I.; Smith, P. A. Dynamic Solid Phase Microextraction for Sampling of Airborne Sarin with Gas Chromatography-Mass Spectrometry for Rapid Field Detection and Quantification. *J. Sep. Sci.* **2004**, *27* (12), 5.
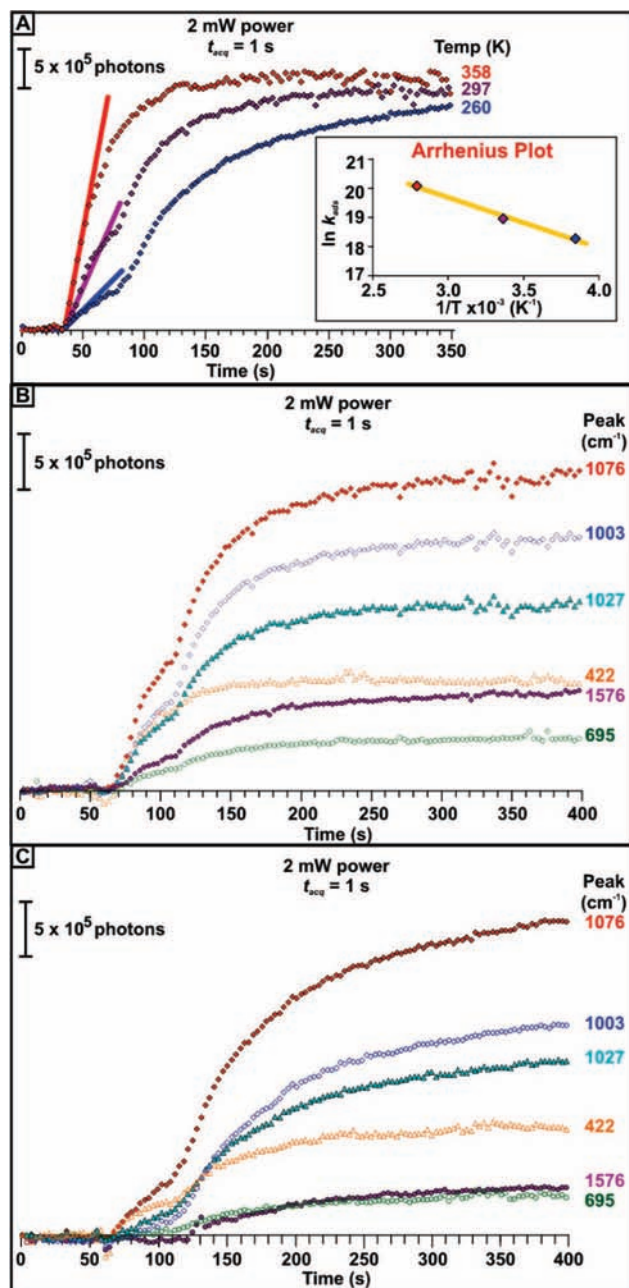
4586 *J. Phys. Chem. A, Vol. 113, No. 16, 2009*

Biggs et al.

(8) Collins, D. C.; Lee, M. L. Developments in Ion Mobility Spectrometry-Mass Spectrometry. *Anal. Bioanal. Chem.* **2002**, *372* (1), 66–73.

(9) Creaser, C. S.; Griffiths, J. R.; Bramwell, C. J.; Noreen, S.; Hill, C. A.; Thomas, C. L. P. Ion Mobility Spectrometry: A Review. Part 1. Structural Analysis by Mobility Measurement. *Analyst* **2004**, *129* (11), 984–994.

(10) Sysoev, A.; Adamov, A.; Vildanoja, J.; Ketoja, R. A.; Kostiainen, R.; Kotiaho, T. Development of an Ion Mobility Spectrometer for use in an Atmospheric Pressure Ionization Ion Mobility Spectrometer-Mass Spectrometer Instrument For Fast Screening Analysis. *Rapid Commun. Mass Spectrom.* **2004**, *18* (24), 3131–3139.

(11) Tang, K.; Shvartsburg, A. A.; Lee, H. N.; Prior, D. C.; Buschbach, M. A.; Li, F. M.; Tolmachev, A. V.; Anderson, G. A.; Smith, R. D. High-Sensitivity Ion Mobility Spectrometry-Mass Spectrometry Using Electrodynamic Ion Funnel Interfaces. *Anal. Chem.* **2005**, *77* (10), 3330–3339.

(12) Zimmermann, S.; Barth, S.; Baether, W. K. M.; Ringer, J. Miniaturized Low-Cost Ion Mobility Spectrometer for Fast Detection of Chemical Warfare Agents. *Anal. Chem.* **2008**, *80* (17), 5.

(13) Christesen, S. D. Raman Cross-Sections of Chemical-Agents and Simulants. *Appl. Spectrosc.* **1988**, *42* (2), 318–321.

(14) Doering, W. E.; Nie, S. M. Spectroscopic Tags using Dye-Embedded Nanoparticies and Surface-Enhanced Raman Scattering. *Anal. Chem.* **2003**, *75* (22), 6171–6176.

(15) Stuart, D. A.; Yonzon, C. R.; Zhang, X. Y.; Lyandres, O.; Shah, N. C.; Glucksberg, M. R.; Walsh, J. T.; Van Duyne, R. P. Glucose Sensing using Near-Infrared Surface-Enhanced Raman Spectroscopy: Gold Surfaces, 10-Day Stability, and Improved Accuracy. *Anal. Chem.* **2005**, *77* (13), 4013–4019.

(16) Sulk, R. A.; Corcoran, R. C.; Carron, K. T. Surface-Enhanced Raman Scattering Detection of Amphetamine and Methamphetamine by Modification with 2-Mercaptonicotinic Acid. *Appl. Spectrosc.* **1999**, *53* (8), 954–959.

(17) Yonzon, C. R.; Haynes, C. L.; Zhang, X. Y.; Walsh, J. T.; Van Duyne, R. P. A Glucose Biosensor Based on Surface-Enhanced Raman Scattering: Improved Partition Layer, Temporal Stability, Reversibility, and Resistance to Serum Protein Interference. *Anal. Chem.* **2004**, *76* (1), 78–85.

(18) Zhang, X. Y.; Young, M. A.; Lyandres, O.; Van Duyne, R. P. Rapid Detection of an Anthrax Biomarker by Surface-Enhanced Raman Spectroscopy. *J. Am. Chem. Soc.* **2005**, *127* (12), 4484–4489.

(19) Carron, K. Surface-Enhanced Raman Studies of Chemically Sensitive Modified Surfaces. *Abst. Pap. Am. Chem. S* **1993**, *206*, 150-COLL.

(20) Gu, B. H.; Tio, J.; Wang, W.; Ku, Y. K.; Dai, S. Raman Spectroscopic Detection for Perchlorate at Low Concentrations. *Appl. Spectrosc.* **2004**, *58* (6), 741–744.

(21) Mosier-Boss, P. A.; Lieberman, S. H. Detection of Nitrate and Sulfate Anions by Normal Raman Spectroscopy and Surface-Enhanced Raman Spectroscopy of Cationic-Coated, Silver Substrates. *Appl. Spectrosc.* **2000**, *54* (8), 1126–1135.

(22) Vo-Dinh, T.; Stokes, D. L. Surface-Enhanced Raman Vapor Dosimeter. *Appl. Spectrosc.* **1993**, *47* (10), 5.

(23) Hill, W.; Wehling, B.; Klockow, D. Analysis of Odorous Vapor Exhaled from Rubber by Surface-Enhanced Raman Scattering. *Appl. Spectrosc.* **1999**, *53* (5), 3.

(24) Stuart, D. A.; Biggs, K. B.; Van Duyne, R. P. Surface-Enhanced Raman Spectroscopy of Half-Mustard Agent. *Analyst* **2005**, *131*, 6.

(25) Taranenko, N.; Alarie, J. P.; Stokes, D. L.; Vo-Dinh, T. Surface-Enhanced Raman Detection of Nerve Agent Simulant (DMMP and DIMP) Vapor on Electrochemically Prepared Silver Oxide Substrates. *J. Raman Spectrosc.* **1996**, *27* (5), 379–384.

(26) Vo-Dinh, T.; Stokes, D. L. Surface-Enhanced Raman Detection of Chemical Vapors with the Use of Personal Dosimeters. *Field Anal. Chem. Technol.* **1999**, *3* (6), 10.

(27) Poirier, G. E.; Pylant, E. D. The Self-Assembly Mechanism of Alkanethiols on Au(111). *Science* **1996**, *272*, 3.

(28) Whelan, C. M.; Smyth, M. R.; Barnes, C. J. HREELS, XPS, and Electrochemical Study of Benzenethiol Adsorption on Au(111). *Langmuir* **1999**, *15*, 10.

(29) Jung, L. S.; Campbell, C. T. Sticking Probabilities in Adsorption of Alkanethiols from Liquid Ethanol Solution onto Gold. *J. Phys. Chem. B* **2000**, *104*, 10.

(30) Karpovich, D. S.; Blanchard, G. J. Direct Measurement of the Adsorption Kinetics of Alkanethiolate Self-Assembled Monolayers on a Microcrystalline Gold Surface. *Langmuir* **1994**, *10*, 7.

(31) Eberhardt, A.; Fenter, P.; Eisenberger, P. Growth Kinetics in Self-Assembling Monolayers: A Unique Adsorption Mechanism. *Surf. Sci.* **1998**, *397*, 5.

(32) Hahner, G.; Woll, C.; Buck, M.; Grunze, M. Investigation of Intermediate Steps in the Self-Assembly of n-Alkanethiols on Gold Surfaces by Soft X-ray Spectroscopy. *Langmuir* **1993**, *9*, 3.

(33) Thomas, R. C.; Sun, L.; Crooks, R. M. Real-Time Measurements of the Gas-Phase Adsorption of n-Alkylthiol Mono- and Multilayers on Gold. *Langmuir* **1991**, *7*, 2.

(34) Schreiber, F.; Eberhardt, A.; Leung, T. Y. B.; Schwartz, P.; Wetterer, S. M.; Lavrich, D. J.; Berman, L.; Fenter, P.; Eisenberger, P.; Scoles, G. Adsorption Mechanisms, Structures, and Growth Regimes of an Archetypal Self-Assembling System: Decanethiol on Au(111). *Phys. Rev. B* **1998**, *57* (19), 4.

(35) Gui, J. Y.; Stern, D. A.; Frank, D. G.; Zapien, D. C.; Hubbard, A. T. Adsorption and Surface Structural Chemistry of Thiophenol, Benzyl Mercaptan, and Alkyl Mercaptans. Comparative Studies at Ag(111) and Pt(111) Electrodes by Means of Auger Spectroscopy, Electron Energy Loss Spectroscopy, Low-Energy Electron Diffraction, and Electrochemistry. *Langmuir* **1991**, *7*, 8.

(36) Wan, L.-J.; Terashima, M.; Noda, H.; Osawa, M. Molecular Orientation and Ordered Structure of Benzenethiol Adsorbed on Gold(111). *J. Phys. Chem. B* **2000**, *104*, 6.

(37) Yang, G.; Liu, G. Y. New Insights for Self-Assembled Monolayers of Organothiols on Au(111) Revealed by Scanning Tunneling Microscopy. *J. Phys. Chem. B* **2003**, *107*, 5.

(38) Rodriguez, L. M.; Gayone, J. E.; Sanchez, E. A.; Grizzi, O.; Blum, B.; Salvarezza, R. C. Room-Temperature Kinetics of Short-Chain Alkanethiol Film Growth on Ag(111) from the Vapor Phase. *J. Phys. Chem. B* **2006**, *110*, 2.

(39) Li, S.; Wu, D.; Xu, X.; Gu, R. Theoretical and Experimental Studies on the Adsorption Behavior of Thiophenol on Gold Nanoparticles. *J. Raman Spectrosc.* **2007**, *38*, 7.

(40) Carron, K. T.; Hurley, L. G. Axial and Azimuthal Angle Determination with Surface-Enhanced Raman Spectroscopy: Thiophenol on Copper, Silver, and Gold Metal Surfaces. *J. Phys. Chem.* **1991**, *95*, 5.

(41) Sandroff, C. J.; Herschback, D. R. Surface-Enhanced Raman Study of Organic Sulfides Adsorbed on Silver: Facile Cleavage of S−S and C−S Bonds. *J. Phys. Chem.* **1982**, *86*, 2.

(42) Agu-Eittah, R. H.; Hilal, R. H. Spectroscopic Studies on Some Benzenethiols. *Appl. Spectrosc.* **1971**, *26* (2), 7.

(43) Haes, A. J.; Haynes, C. L.; McFarland, A. D.; Schatz, G. C.; Van Duyne, R. P.; Zou, S. L. Plasmonic Materials for Surface-Enhanced Sensing and Spectroscopy. *MRS Bull.* **2005**, *30* (5), 368–375.

(44) Stiles, P.; Dieringer, J.; Shah, N. C.; Van Duyne, R. P. Surface-Enhanced Raman Spectroscopy. *Annu. Rev. Anal. Chem.* **2008**, *1*, 5.

(45) McCreery, R. L., *Raman Spectroscopy for Chemical Analysis*; John Wiley and Sons, Inc.: New York, 2000; Vol. 157.

(46) Petty, C. J.; Hendra, P. J.; Jawhari, T. *Spectrochim. Acta* **1991**, *47A*, xxx.

(47) Moskovits, M. Surface Selection Rules. *J. Chem. Phys.* **1982**, *77* (9), 7.

(48) King, F. W.; Van Duyne, R. P.; Schatz, G. C. Theory of Raman Scattering by Molecules Adsorbed on Electrode Surfaces. *J. Chem. Phys.* **1978**, *69* (10), 9.

(49) Haynes, C. L.; Van Duyne, R. P. Plasmon-Sampled Surface-Enhanced Raman Excitation Spectroscopy. *J. Phys. Chem. B* **2003**, *107* (30), 7426–7433.

(50) Schwartz, P.; Schreiber, F.; Eisenberger, P.; Scoles, G. Growth Kinetics of Decanethiol Monolayers Self-Assembled on Au(111) by Molecular Beam Deposition: An Atomic Beam Diffraction Study. *Surf. Sci.* **1999**, *423*, 17.

(51) Dubois, L. H.; Zegarski, B. R.; Nuzzo, R. G. Molecular Ordering of Organosulfur Compounds on Au(111) and Au(100): Adsorption from Solution and in Ultrahigh Vacuum. *J. Chem. Phys.* **1992**, *98* (1), 10.

(52) Garcia-Vidal, F. J.; Pendry, J. B. Collective Theory for Surface-Enhanced Raman Scattering. *Phys. Rev. Lett.* **1996**, *77* (6), 5.

(53) Xu, H. X.; Aizpurua, J.; Käll, M.; Apell, P. Electromagnetic Contributions to Single-Molecule Sensitivity in Surface-Enhanced Raman Scattering. *Phys. Rev. E* **2000**, *62* (3), 4318–4324.

(54) Weinberg, W. H.; Grunze, M.; Kreuzer, H. J. *Kinetics of Interface Reactions*; Springer: Berlin, 1987.

(55) McQuarrie, D. A.; Simon, J. D. *Physical Chemistry: A Molecular Approach*; University Science Books: Sausalito, 1997.